Joint Inversion of Airborne Electromagnetic and Total Magnetic Intensity Data Using Gramian Structural Constraints

M. Jorgensen[1,2], L. Cox[1], M. Zhdanov[1,2]

[1] TechnoImaging; [2] University of Utah

Summary

Airborne electromagnetic (AEM) and total magnetic intensity (TMI) data are combined in a joint Gramian inversion to obtain structurally-similar 3D resistivity and susceptibility models of a subset of the Reid-Mahaffy test site in Ontario, Canada. Spatially limited structural constraints are enforced through a correlation of the model gradients. Frequency-domain AEM data are sensitive to shallow resistivity structure, while TMI data are more sensitive to deeper structure. By combining these complementary data, the jointly inverted models provide a more consistent image of the geologic structure of the area, simplifying interpretation.

Introduction

Geologic interpretation of 3D physical property models inverted from various geophysical data for mineral exploration can be complicated by various factors. These complications can be overcome by jointly inverting different geophysical data sets. Total magnetic intensity (TMI) data is generally gathered in airborne electromagnetic (AEM) surveys, making the pair a natural choice for joint inversion.

Our approach to addressing this problem is joint inversion with spatially limited Gramian constraints (Zhdanov et al., 2012; Zhdanov, 2015), enforcing structural correlation of the gradients of different physical property models. As an illustration of this approach, we present the results of inverting the frequency-domain DIGHEM AEM and airborne magnetic data collected over the Reid-Mahaffy test site in Ontario, Canada (Reford and Fyon, 2000). The inversion workflow consists of filtering the TMI data, obtaining a 1D standalone resistivity inverse model to determine the general earth structure, and then obtaining 3D standalone resistivity and susceptibility inverted models to determine optimal parameters for the joint inversion. For areas with strongly conductive overburden, the Gramian constraint is only applied below conductive overburden. This increases the speed of convergence and avoids spurious near surface inhomogeneities in the susceptibility model.

We present the resistivity and magnetic susceptibility models of a subset of the Reid-Mahaffy test site obtained from both standalone and joint Gramian 3D inversions. A geologically meaningful susceptibility model was produced by the joint inversion, while honouring the data. Joint Gramian inversion provides anomalies with the sharper boundaries, stronger structural correlations, and with the same level of data misfit as the standalone inversions.

Theory

The geophysical inverse problem is given by the operator equations $m^i = \left(A^i\right)^{-1} d^i$, $(i = 1,2)$, where m^i are the models, A^i are the forward modelling operators, d^i are the data, and the superscript $i = 1,2$ indicates the electromagnetic and magnetic problems, respectively. The solutions of these inverse problems are usually poorly conditioned, so we apply the regularization and minimize a parametric functional using the conjugate gradient method (Zhdanov 2009; 2015).

Separate misfit and smoothing terms, corresponding to the TMI and EM data, are combined in the joint parametric functional and subject to the spatially limited Gramian constraint:

$$P = \sum_{i=1}^{2} \varphi\left(m^i\right) + \alpha \sum_{i=1}^{2} s\left(m^i\right) + \beta G\left(\nabla m^i\right). \quad (1)$$

The misfit terms are defined as follows,

$$\varphi\left(m^i\right) = \left\| W_d^i \left(A^i\left(m^i\right) - d^i\right)\right\|_2^2, \quad (2)$$

where W_d^i are the data weights, $A^i\left(m^i\right)$ are the predicted data, and d^i are the observed data. The stabilizing terms are defined as follows,

$$s\left(m^i\right) = \left\| W_m^i \left(m^i - m_{apr}^i\right)\right\|_2^2, \quad (3)$$

where W_m^i are the model weights and m_{apr}^i are the a priori models.
The Gramian term is defined by the following formula,

$$G\left(\nabla m^i\right) = \begin{vmatrix} \left(\nabla m^1, \nabla m^1\right) & \left(\nabla m^1, \nabla m^2\right) \\ \left(\nabla m^2, \nabla m^1\right) & \left(\nabla m^2, \nabla m^2\right) \end{vmatrix}, \quad (4)$$

where ∇m^i are the gradients of the models, and $(*,*)$ denotes the inner product (Zhdanov, 2015). As this determinant is minimized, the model gradients are aligned enforcing structural similarity. The process is similar to the cross-gradients approach (Gallardo and Meju, 2003); however, the Gramian constraint allows an exact analytical formula for the gradient direction of the parametric functional, without any approximation typical for the cross-gradients approach, which ensures rapid convergence.

Both TMI and AEM data are weighted by a function of the errors:

$$W_d^i = 1/\left(e_{\%}^i d^i + e_{abs}^i\right), \quad (5)$$

where $e_{\%}^i$ are the percent errors (5% for the AEM data and 5% for the TMI data), and e_{abs}^i are the absolute error floors (0.1-10 ppm for the AEM data and 2 nT for the TMI data). Data weights are then further scaled in the joint inversion such that the first misfit for each term $\varphi\left(m^i\right)$ is equal to 1. Model weights are determined by the following function of the sensitivity:

$$W_m^i = diag\sqrt[4]{F^{i*}F^i}, \quad (6)$$

where F^i is the Fréchet derivative of $A^i\left(m^i\right)$, and F^{i*} is the complex conjugate. Model weights are then further scaled in the joint inversion by normalizing by the maximum value of the model parameters obtained from standalone inversions.

The regularization terms α, β are adaptively reduced to ensure stable convergence (Zhdanov, 2009; 2015). The inversion is halted when the χ^2 fit corresponding to both misfit terms drops to 1, meaning we have reached the interpreted noise level.

Results

We inverted the data collected over a subdomain of the test site shown in Figure 1, where the data demonstrated both conductive and magnetic anomalies. Borehole information (Reford and Fyon, 2000) for this target indicates conductive overburden to a depth of ~50 m, underlain by layers of intrusive intermediate and felsic rocks and a strongly fractured graphitic ultramafic intrusion. TMI data were filtered to eliminate responses from the deeper sources. Despite filtering, the standalone inverted susceptibility model (Figure 2) resolved a plate like feature at the bottom of the domain, corresponding to a layer of intermediate and felsic volcanics underlying the ultramafic intrusion, complicating interpretation.

We contrast the standalone inverted models with the jointly inverted models (Figure 3), which have sharper boundaries, more structural correlation, and lack the spurious plate at the bottom of the domain present in the standalone susceptibility model.

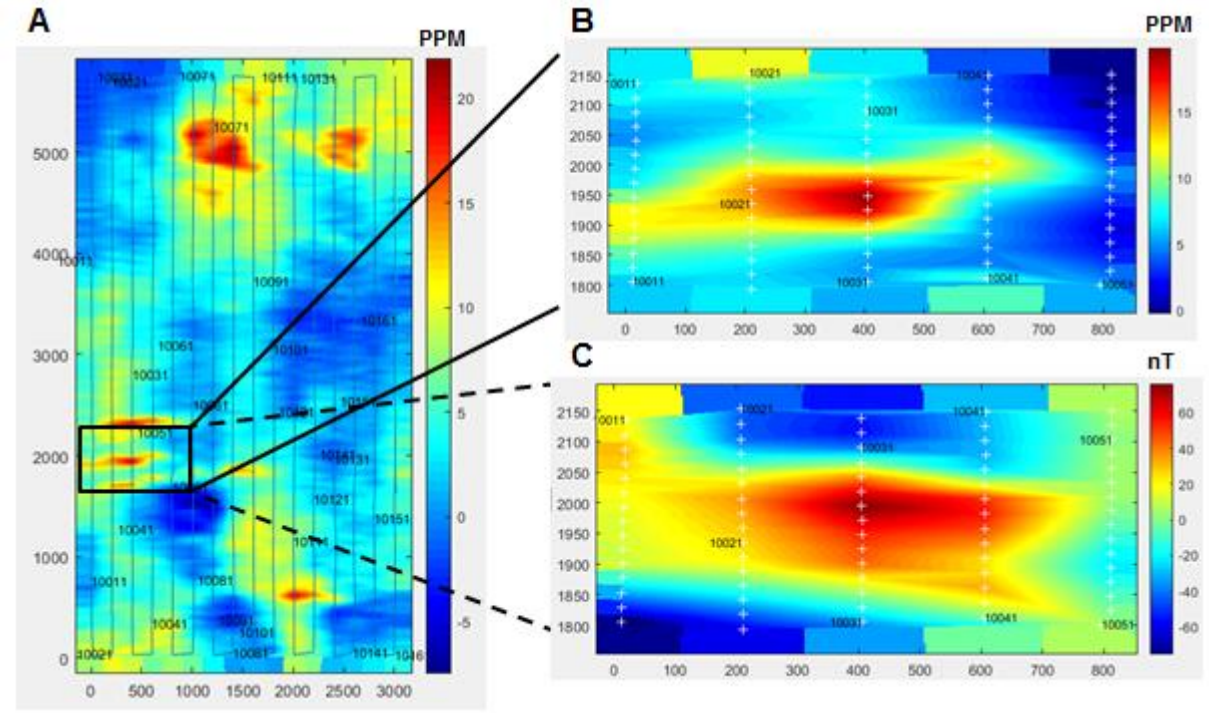

Figure 1 *Panel (A) shows the full Reid-Mahaffy test site 1068 Hz DIGHEM data map shown in local coordinates. Panel (B) shows the 1068 Hz DIGHEM data map over the inversion domain. Panel (C) shows the filtered TMI data map over the inversion domain.*

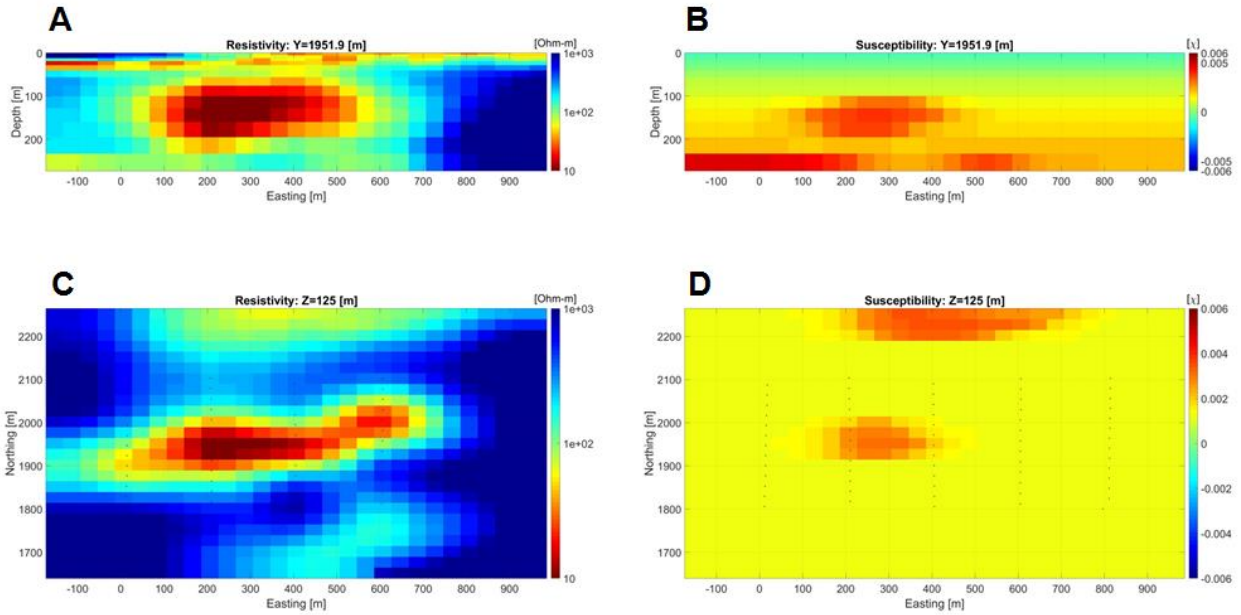

Figure 2 *Panels (A) & (B) show cross-line vertical sections of the standalone inverted resistivity and susceptibility models, respectively. Panels (C) & (D) show horizontal sections of the standalone inverted resistivity and susceptibility models, respectively.*

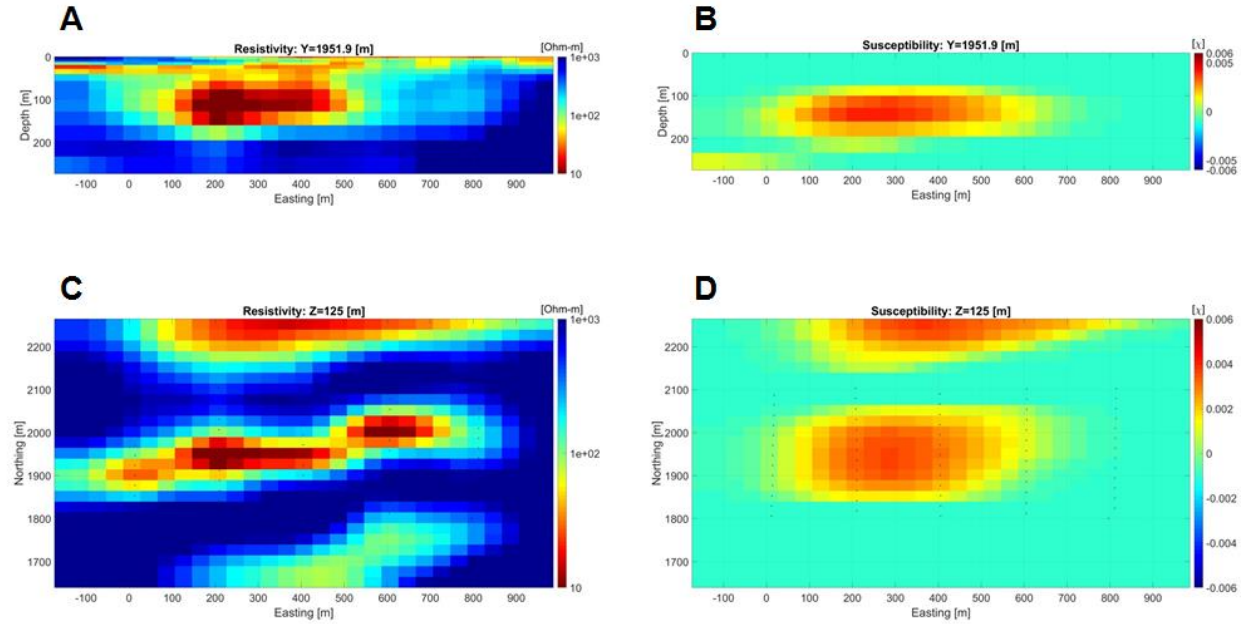

Figure 3 *Panels (A) & (B) show cross-line vertical sections of the jointly inverted resistivity and susceptibility models, respectively. Panels (C) & (D) show horizontal sections of the jointly inverted resistivity and susceptibility models, respectively.*

The cross plots of susceptibility and log conductivity shown in Figure 4 indicate the level of structural correlation. The nebulous cloud representing the standalone inverted models indicates minimal correlation, making interpretation difficult. Conversely, the parabolic trend representing the jointly inverted models, combined with sharper geospatial boundaries and target coincidence, can significantly ease interpretation.

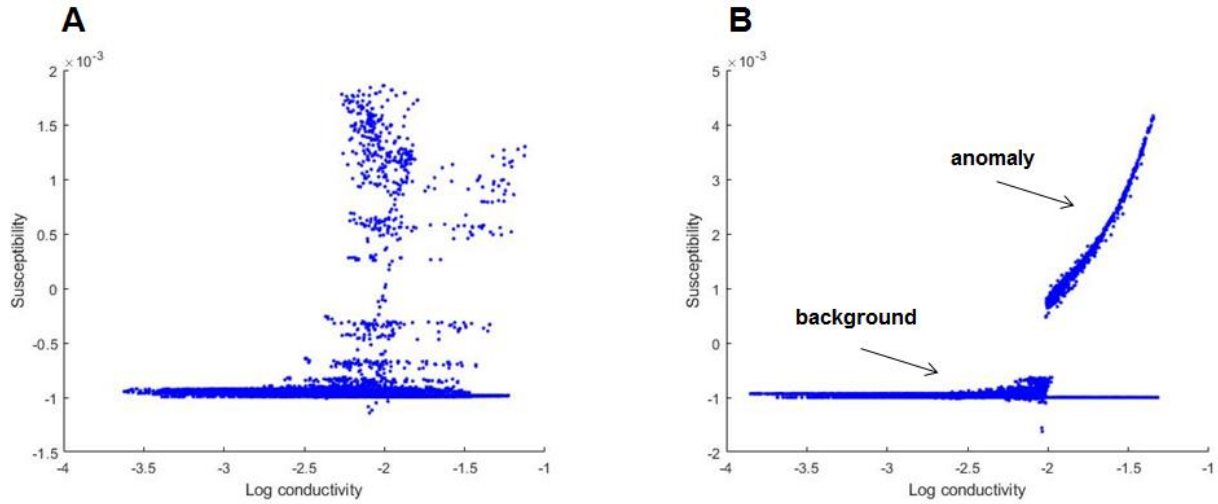

Figure 4 *Panels (A) & (B) show property cross plots of susceptibility and log conductivity for the standalone inverted models and jointly inverted model, respectively. The jointly inverted models show enhanced structural correlation of the target.*

Conclusions

We have introduced a method of joint inversion of AEM and TMI data using Gramian structural constraints. We have jointly inverted frequency-domain DIGHEM and airborne magnetic data gathered over the Reid-Mahaffy test site. Comparison of the standalone inverted resistivity and susceptibility models versus the joint inverted models, which all have the same level of data misfit ($\chi^2 = 1$), demonstrates that the jointly inverted models can recover the more compact bodies, more structural correlation, and more geologically reasonable models than the standalone inverse solutions.

Acknowledgements

The authors would like to thank CEMI and TechnoImaging for their support. The AEM and TMI data were collected by Fugro and made available by the Ontario Geological Survey, Canada

References

Gallardo, L.A. and Meju, M.A. [2003]. Characterization of heterogeneous near-surface materials by joint 2D inversion of DC resistivity and seismic data. *Geophysical Research Letters*, **30**(13), 1658.

Reford, S.W. and Fyon, A. [2000]. *Airborne magnetic and electromagnetic surveys, Reid-Mahaffy airborne geophysical test site survey, miscellaneous release—Data (MRD) 55, geological setting, measured and processed data, and derived products* .Published report. http://www.geologyontario.mndm.gov.on.ca/mndmfiles/pub/data/imaging/MRD055/MRD055.pdf.

Zhdanov, M.S., Gribenko, A.V. and Wilson, G. [2012]. Generalized joint inversion of multimodal geophysical data using Gramian constraints. *Geophysical Research Letters*, **39** (9).

Zhdanov, M.S. [2009]. *Geophysical Electromagnetic Theory and Methods.* Elsevier.

Zhdanov, M.S. [2015]. *Inverse Theory and Applications in Geophysics.* Elsevier.